A novel compact microstrip phase shifter for microstrip antenna arrays

M. G. ȚURCAN*
Military Technical Academy „Ferdinand I", Faculty of Communications and Electronics Systems for Defence and Security, 39-49 George Coșbuc Blvd., 050141, Bucharest, Romania

A novel simplified phase shifter to equip microstrip antenna arrays is demonstrated in the article. The proposed phase shifter include three transmission lines placed around a probe excitation base. With this compact design, a particular antenna array is capable of steering the main beam towards five predetermined directions. To show the advantages of the proposed phase shifter, four models are used to build the excitation circuit of a linear array of four cylindrical dielectric resonator antennas, with a dielectric constant of 34. The implemented practical model has obtained a maximum steering angle of 36 degrees. The paper shows an excellent matching between simulations and measurements.

(Received July 10, 2023; accepted August 10, 2023)

Keywords: Microstrip phase shifter, Steering angle, Main beam, Cylindrical dielectric resonator antenna array

1. Introduction

Phased array antennas are used on a wide range of applications like: space communications [1], military radars [2], Wi-Fi and LTE technology [3] or health care applications [4].

In the last decade the beam steering has been studied by many researchers [5-7]. The beam steering of an antenna array can be accomplished by changing the phases of the radio frequency signals of the elements [8]. This can be done with phase shifters. The mechanical phase shifter can be expensive and bulky so, to reduce the price and the size of the antenna arrays, electronic phase shifters are used.

In this paper, a compact phase shifter for a linear array of four cylindrical dielectric resonator antennas, at 5.35 GHz, is designed. The trend in mobile communication/Wi-Fi systems is to reduce the size of mobile terminals. The goal of this study is to design a phase shifter small enough, which could successfully replace the conventional 2-bit phase shifter and provide 3 distinct phases. The phase shifter proposed in this paper is more compact that the one (with 2-bit) presented in [9], and it is capable of steering the main beam of the antenna array towards five predetermined directions.

2. Experimental

In Fig. 1 is presented the geometric configuration of a linear array of four cylindrical dielectric resonator antenna.

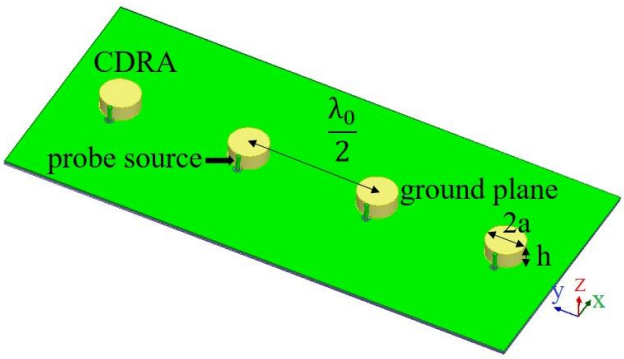

Fig. 1. Linear array of four CDRA array geometry – top view (color online)

The array elements are made of advanced materials, having dielectric constant ε_r = 34, radius a = 4.55 mm and height h = 3.7 mm. They are fixed with a thin layer of low permittivity glue on a Rogers 4003 grounded substrate, of length 50 mm and width 120 mm, with dielectric constant ε_s = 3.55 and thickness t = 0.813 mm, and separated by a half of free-space wavelength at the resonant frequency.

The resonance frequency of resonators is 5.51 GHz [10, 11].

Four probe excitations of 1 mm diameter and height equal to that of the resonators are located adjacent to them and will excite the fundamental $HE_{11\delta}$ mode.

To steer the antenna beam in a desired direction, the phase of each element of the array must be changed. This can be achieved by delaying an input signal by increasing the transmission line length.

The phase shifters design is shown in Fig. 2.

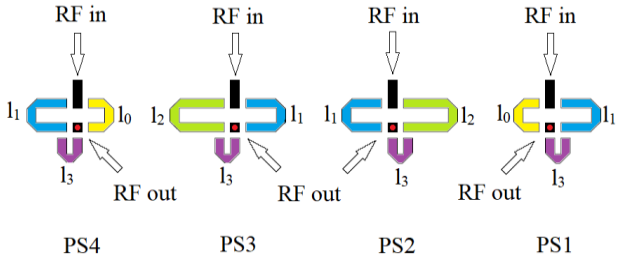

Fig. 2. Phase shifters design (color online)

As shown in Fig. 2, a single phase shifter include three transmission lines placed around a probe excitation base. Each of the traces are connected to the probe excitation and can be switched to provide different phase shifts. The gap between the transmission lines is 1.2 mm. For simulation purpose, a lumped component will be placed in each gap to connect the transmission lines, in order to provide the effect of a switch, and to obtain the desired phase shift.

According to [12] the differential phase shift between two transmission lines (l_1 and l_2) is:

$$\Delta\phi = \frac{2\pi}{\lambda_0}\sqrt{\varepsilon_{eff}} \times (l_2 - l_1) \quad (1)$$

where ε_{eff} is effective microstrip permittivity.

The differences between the delay lines lengths and the reference line (l_0), is shown in Table 1.

Table 1. The differences between the delay lines lengths and the reference line

No.	ΔØ	ΔL	Length
1	60°	l_1-l_0	5.61 mm
2	120°	l_2-l_0	11.22 mm
3	180°	l_1+l_3-l_0	16.83 mm
4	240°	l_2+l_3-l_0	22.44 mm

A corporate feed network, as shown in Fig. 3, is used to transfer the input power to antennas.

It consists of six quarter-wave impedance transformers, to provide a good matched feeding network [14], and mitered transmission lines, in order to minimize reflection losses due to sharp corners [15].

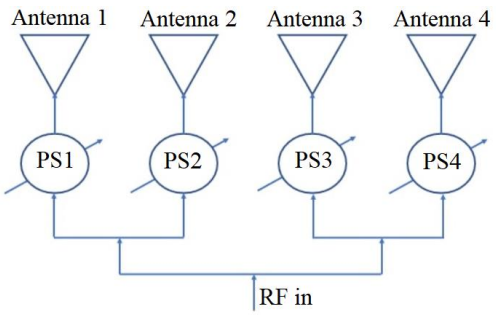

Fig. 3. A corporate feed network design for a four-element linear array antenna (color online)

The geometric configuration of the corporate feed network connected to phase shifters for the proposed antenna array is shown in Fig. 4. SW_{ij} with i = {1, 2, 3, 4}, j = {1, 2, 3, 4, 5, 6} are lumped components with switch effect.

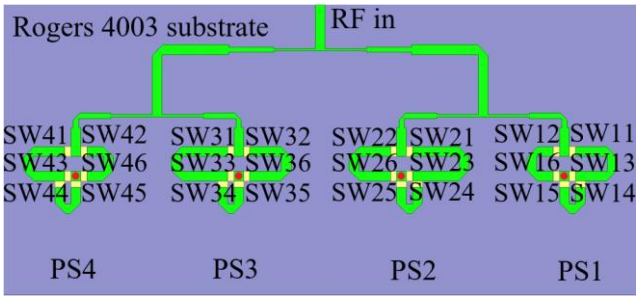

Fig. 4. A corporate feed network with phase shifters for a four linear antenna array – bottom view (color online)

In order to obtain the desire phase shift, the states of the switches are changed from ON to OFF and vice-versa.

The microstrip lines combinations, for each phase shifter, are shown in Table 2.

Table 2. Microstrip lines combination for each phase shifter

Phase shift combination	Microstrip line combination			
	PS1	PS2	PS3	PS4
0°-240°-120°-0°	l_0	l_2+ l_3	l_2	l_0
180°-120°-60°-0°	l_1+ l_3	l_2	l_1	l_0
0°-0°-0°-0°	l_1	l_1	l_1	l_1
0°-60°-120°-180°	l_0	l_1	l_2	l_1+ l_3
0°-120°-240°-0°	l_0	l_2	l_2+ l_3	l_0

High Frequency Structural Simulator (HFSS) was employed to carry out the simulations.

When the combination of phases is 0°-0°-0°-0°, the gain of the antenna array is 11.51 dB. The reflection coefficient |S11| is - 26.5 dB, at resonant frequency of 5.35 GHz (Fig. 5).

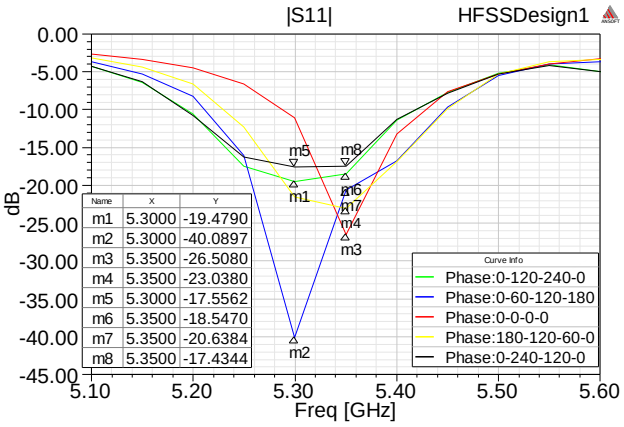

Fig. 5. Reflection coefficient |S11| of the antenna array depending on the combination of phases (color online)

Depending on the combination of phases, the steering angle are: - 36º, - 16º, 0º, + 16º and + 35º. They can be seen from radiation pattern of the antenna array on Fig. 6.

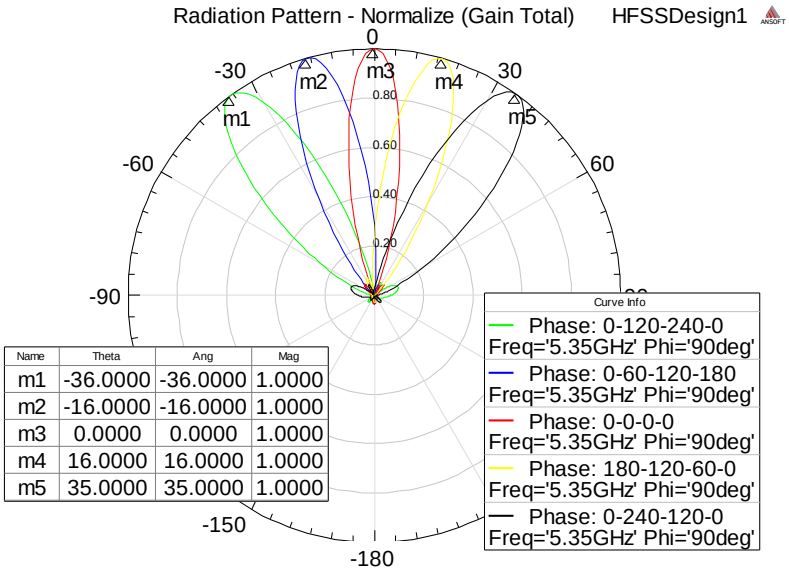

Fig. 6. Radiation pattern of the antenna array depending on the combination of phases (color online)

As shown in Fig. 5, the resonant frequency of the array changes to 5.3 GHz, when the combinations of phases are 0º-60º-120º-180º, 0º-120º-240º-0º and 0º-240º-120º-0º respectively.

The reflection coefficient, at the frequency of 5.35 GHz is: – 20.63 dB, for the phase shift 0º-60º-120º-180º, - 18.54 dB, for the phase shift 0º-120º-240º-0º, and – 17.43 dB, for the phase shift 0º-240º-120º-0º respectively. These results can be improved if each trace of transmission line, from phase shifter, is matched to 50 Ω impedance. One solution for this is to use a short open stub, as can be seen in Fig. 7 (they are colored in yellow, black, blue and red.). This figure shows the dimensions of the updated corporate feed network with phase shifters and dimensions of the stubs.

The new simulation results: reflection coefficient, gain and radiation pattern are plotted in Figs 8-10. The results are centralized in Table 3.

After making these changes, the resonance frequency is equal to 5.35 GHz, for each individual case. Unfortunately, for the phase shift combination 0º-0º-0º-0º the reflection coefficient value decreased slightly, causing a higher VSWR than the first situation. This circumstance can be improved by a better matching to 50 Ω microstrip line.

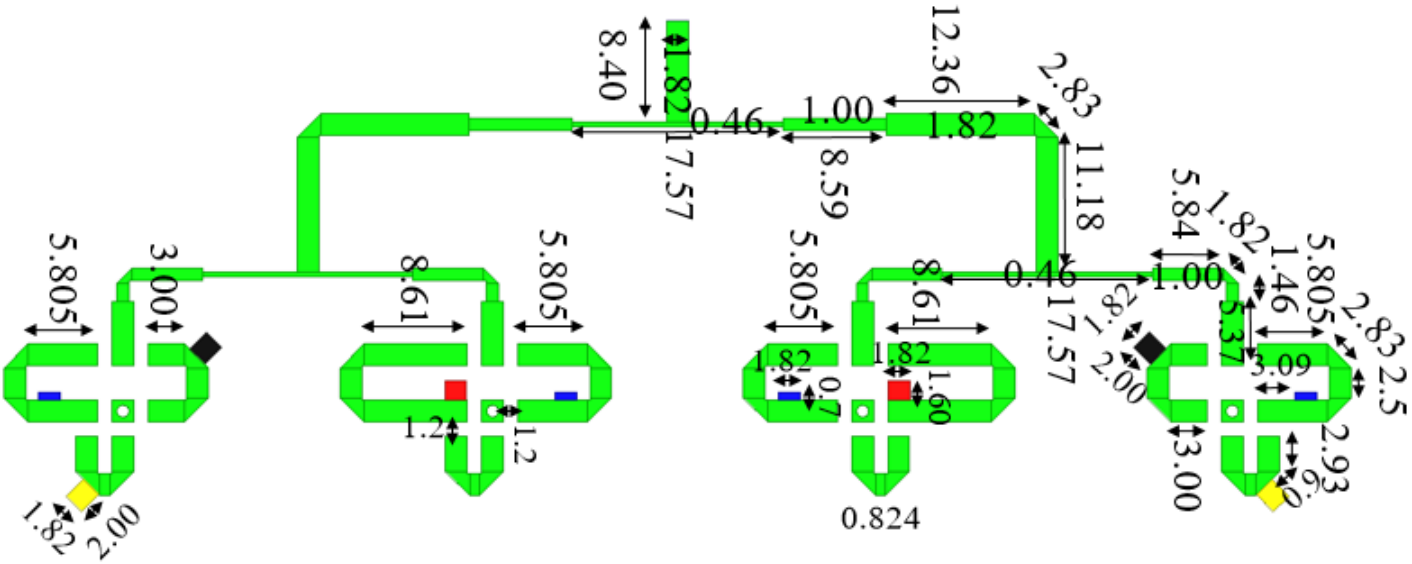

Fig. 7. Updated corporate feed network with phase shifters for a four-element linear array antenna – bottom view (color online)

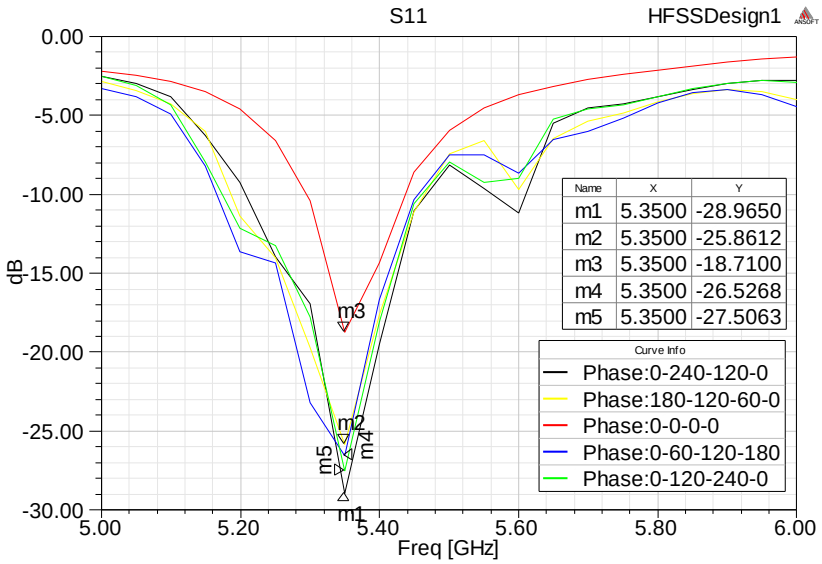

Fig. 8. Reflection coefficient |S11| for updated corporate feed network (color online)

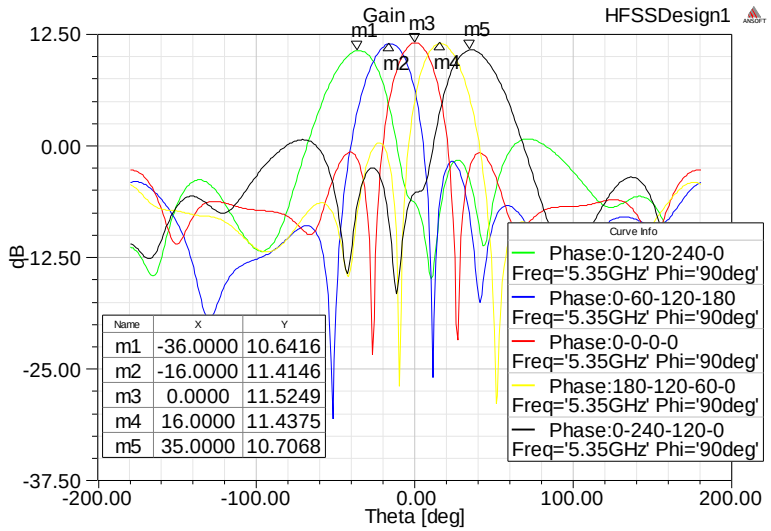

Fig. 9. Gain for updated corporate feed network (color online)

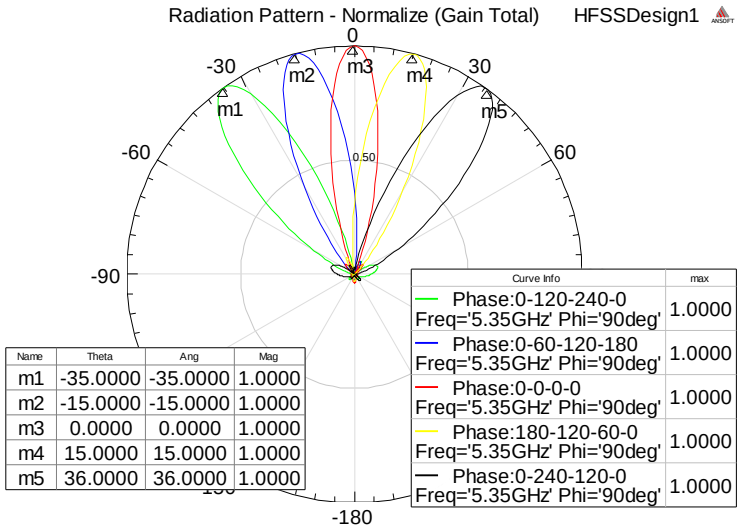

Fig. 10. Radiation pattern for updated corporate feed network (color online)

Table 3. Array parameters depending on the combination of phases

Phase shift	Steering angle (degree)	f_0 (GHz)	|S11| (dB)	-3 dB angle (degree)	-10 dB bandwidth (MHz)	VSWR	Gain (dB)	Difference between lobes (dB)	Radiation Efficiency (%)
0º-120º-240º-0º	-35	5.35	-27.5	29.16	287.3	1.08	10.76	9.70	93.65
0º-60º-120º-180º	-15	5.35	-26.52	26.16	290	1.09	11.29	11.85	95.05
0º-0º-0º-0º	0	5.35	-18.71	23.08	144	1.26	11.53	12.24	95.70
180º-120º-60º-0º	+15	5.35	-25.86	25.51	278.2	1.10	11.29	10.89	94.81
0º-240º-120º-0º	+36	5.35	-28.96	29.48	260	1.07	10.73	9.71	93.22

3. Results

The fabricated prototype of antenna array is shown in Fig. 11. The Anritsu VNA MS2026C vector analyzer was used to measure the reflection coefficient. The results are plotted in Fig. 12.

The AVG POWER SENSOR NRP-Z221 was used to measure the radiated power radiation pattern of the antenna array. The results are plotted in Fig. 13.

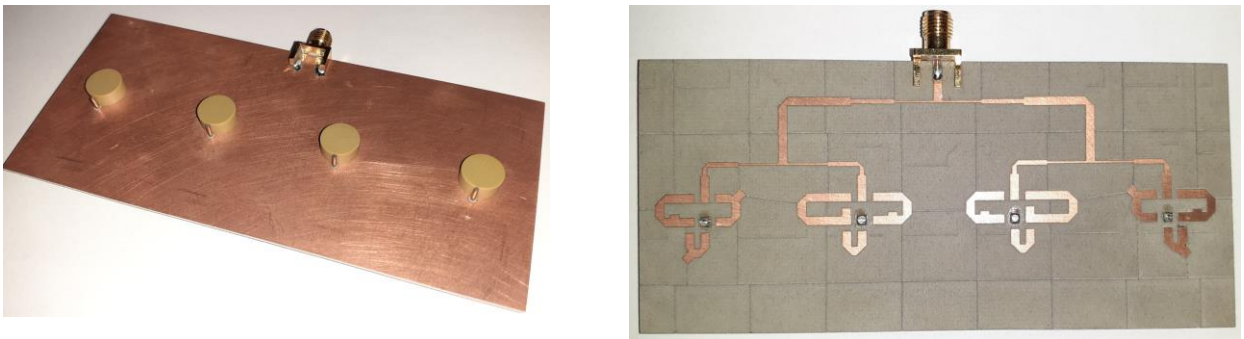

(a) *(b)*

Fig. 11. A prototype of the fabricated antenna array. (a) Top view. (b) Bottom view (color online)

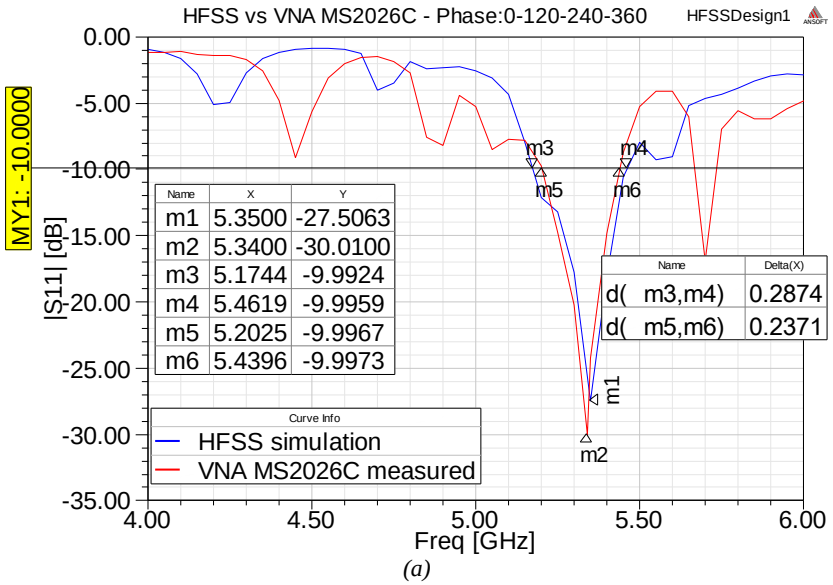

(a)

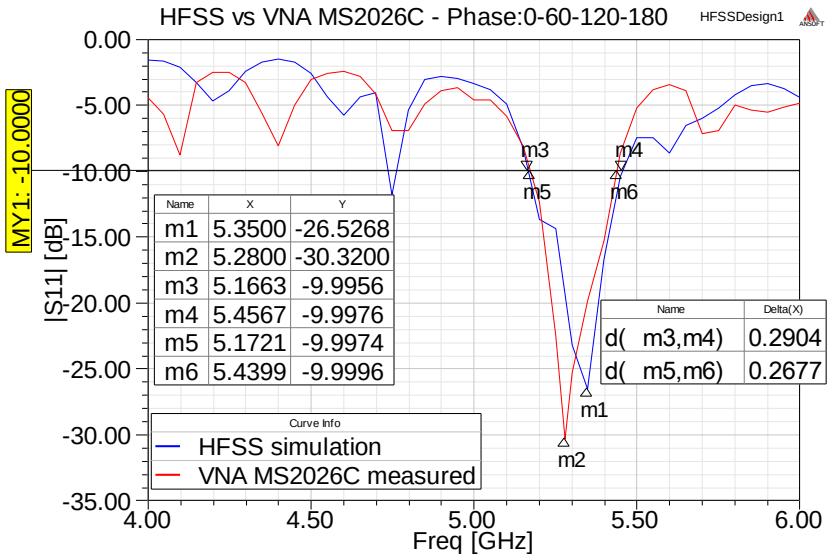
HFSS vs VNA MS2026C - Phase:0-60-120-180
HFSSDesign1
MY1: -10.0000
|S11| [dB]
Freq [GHz]
Name X Y
m1 5.3500 -26.5268
m2 5.2800 -30.3200
m3 5.1663 -9.9956
m4 5.4567 -9.9976
m5 5.1721 -9.9974
m6 5.4399 -9.9996
Name Delta(X)
d(m3,m4) 0.2904
d(m5,m6) 0.2677
Curve Info
HFSS simulation
VNA MS2026C measured

(b)

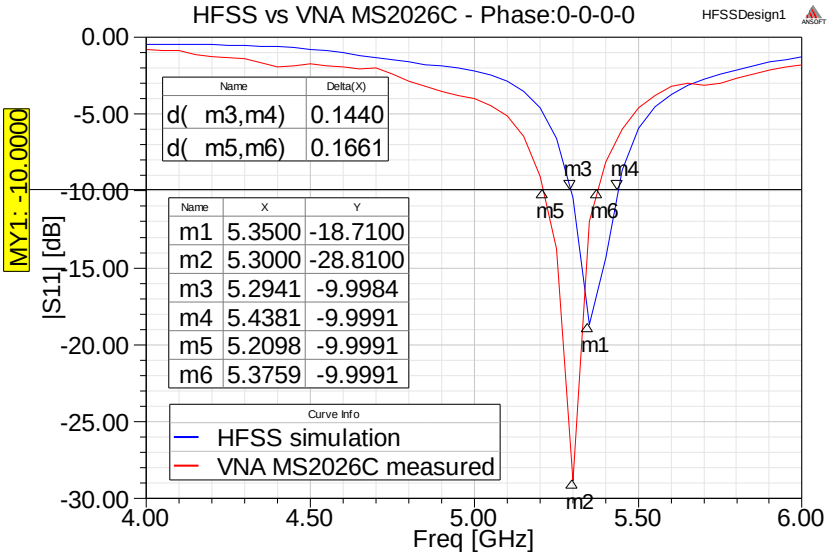
HFSS vs VNA MS2026C - Phase:0-0-0-0
HFSSDesign1
MY1: -10.0000
|S11| [dB]
Freq [GHz]
Name Delta(X)
d(m3,m4) 0.1440
d(m5,m6) 0.1661
Name X Y
m1 5.3500 -18.7100
m2 5.3000 -28.8100
m3 5.2941 -9.9984
m4 5.4381 -9.9991
m5 5.2098 -9.9991
m6 5.3759 -9.9991
Curve Info
HFSS simulation
VNA MS2026C measured

(c)

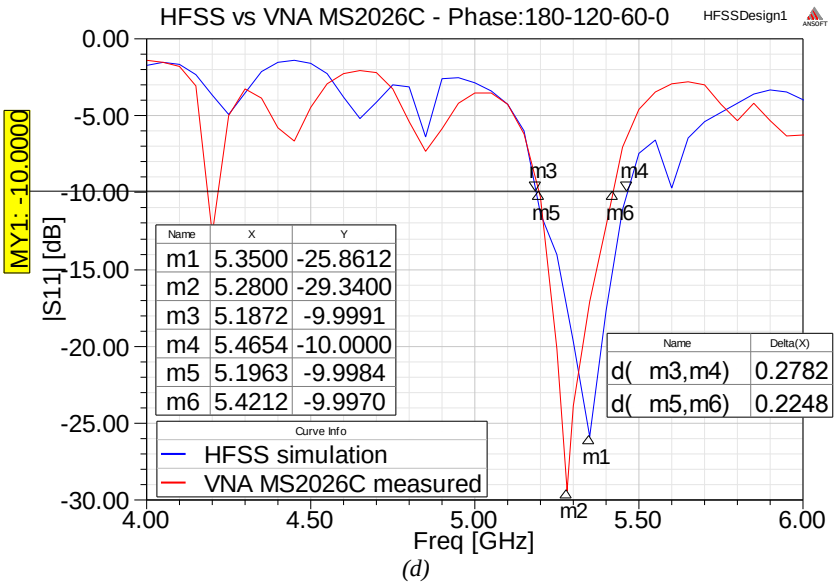
HFSS vs VNA MS2026C - Phase:180-120-60-0
HFSSDesign1
MY1: -10.0000
|S11| [dB]
Freq [GHz]
Name X Y
m1 5.3500 -25.8612
m2 5.2800 -29.3400
m3 5.1872 -9.9991
m4 5.4654 -10.0000
m5 5.1963 -9.9984
m6 5.4212 -9.9970
Name Delta(X)
d(m3,m4) 0.2782
d(m5,m6) 0.2248
Curve Info
HFSS simulation
VNA MS2026C measured

(d)

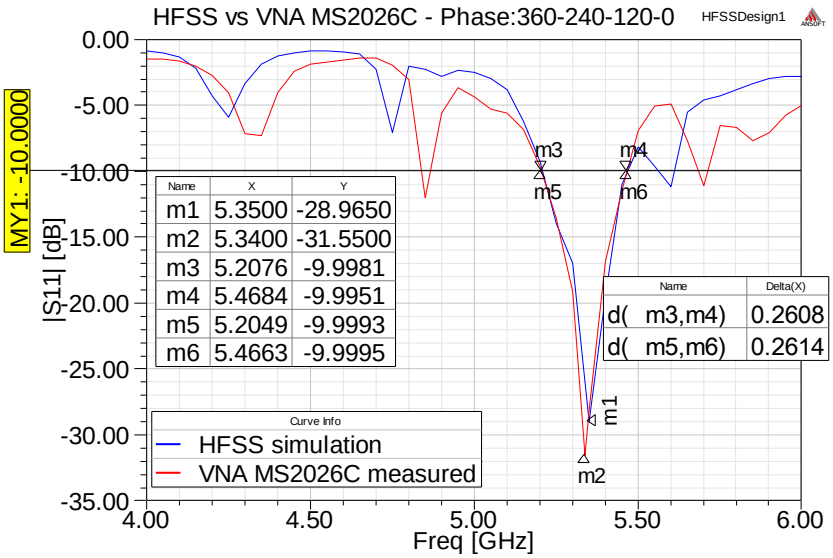

(e)

Fig. 12. Simulated vs. measured reflection coefficient |S11| for various cases

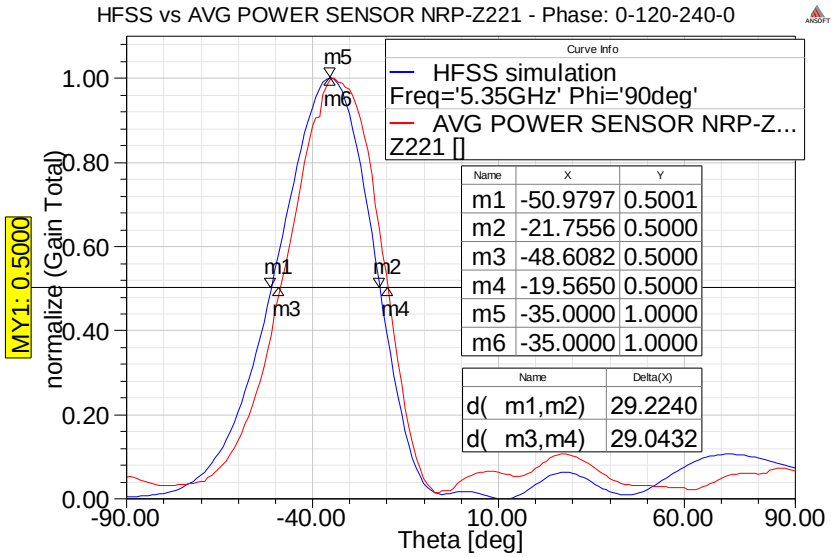

(a)

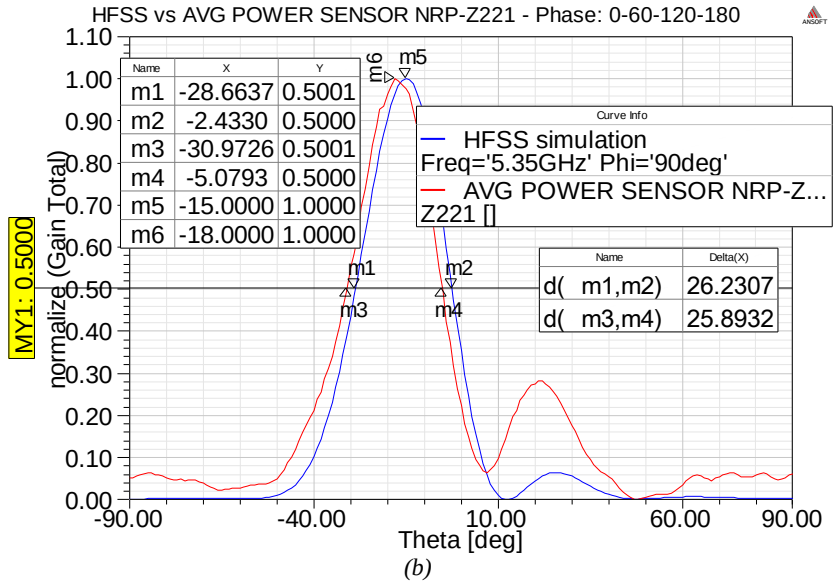

(b)

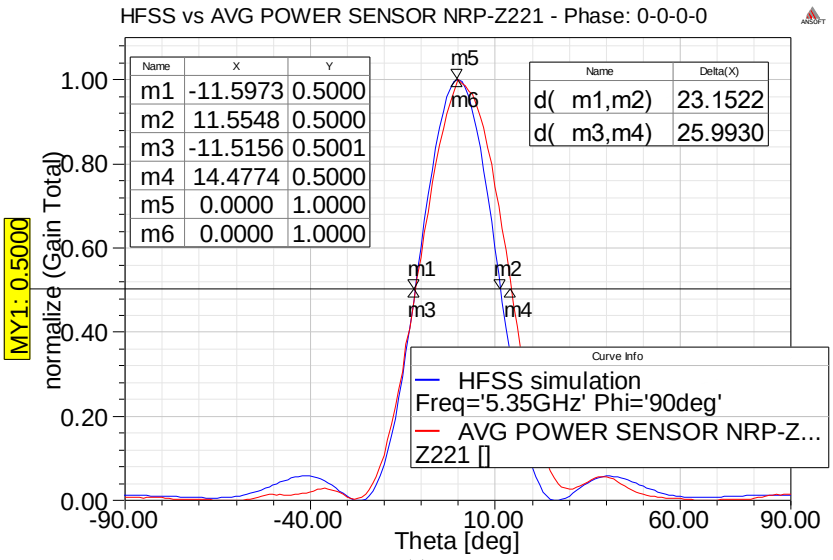

(c)

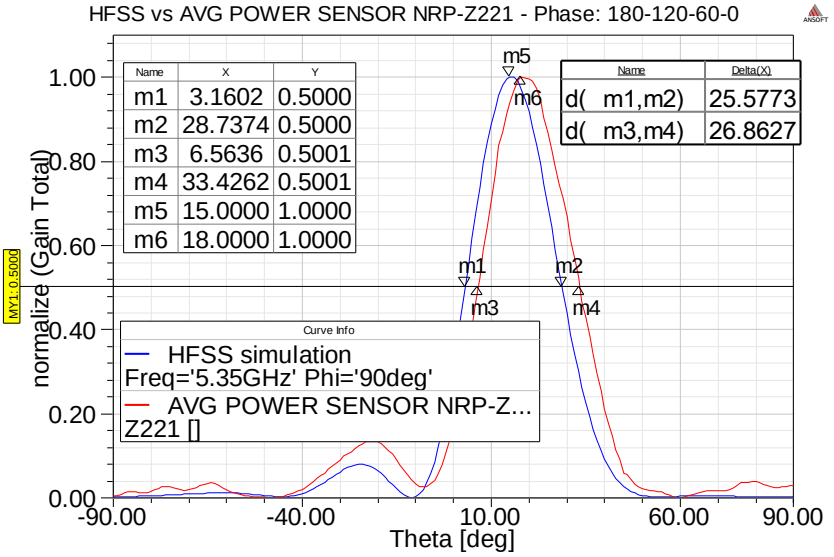

(d)

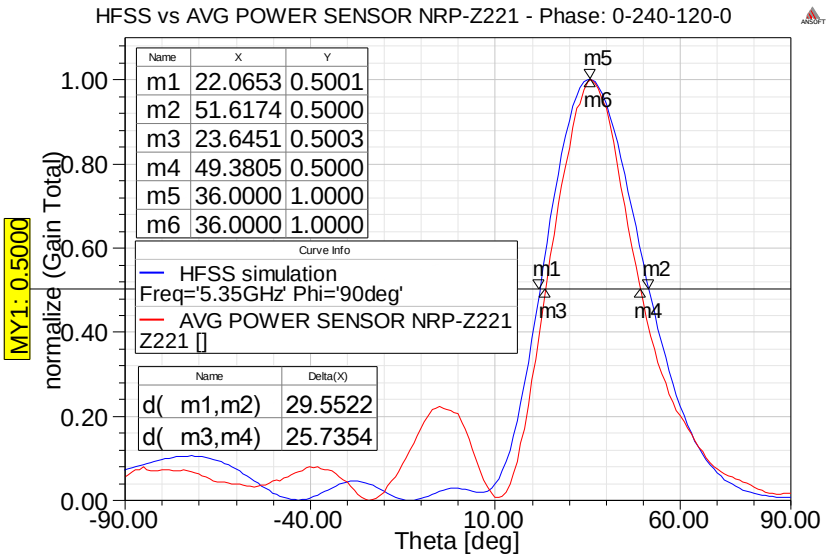

(e)

Fig. 13. Simulated vs. measured normalized radiation pattern

4. Discussions

The |S11| plot, from Fig. 12, shows an excellent matching between simulations and measurements.

The differences are minor, the resonance frequency changing from 5.35 GHz to: 5.3 GHz, for the phase shift 0^o-0^o-0^o-0^o, 5.28 GHz for the phase shift 0^o-60^o-120^o-180^o and 180^o-120^o-60^o-0^o, and 5.34 GHz for the rest. Also, the measured bandwidth is approximately equal to the simulated bandwidth, with deviations of -17.5% (case a), -7.81% (case b), +11.53% (case c), -19.19% (case d), and + 0.23% (case e). The measured reflection coefficients for all cases are from -28.81 dB to -31.55 dB.

As shown in Fig. 13, the measured radiation pattern and to the simulated one, are almost identical. The steering angles of the manufactured antenna array are: - 35^o, - 18^o, 0^o, + 18^o and + 36^o. For each case the gain is greater than 10 dB. The difference between main lobe and sidelobes is at least 9.7 dB. The fabricated antenna array is very directive with measure values for - 3 dB angle, from 24.89 to 29.04 degree.

The radiation efficiency of the CDRA array is very high, with values over 93 %.

As we can see, there are some minor differences between the simulated and the measured values.

These differences can be explained by the following factors:

- imperfect connection between the probe excitation and microstrip line;
- the excess material resulting from connecting the probe excitation to microstrip line;
- the practical probe excitation length is different from the theoretical one;
- imperfect coupling between probe excitation and dielectric resonator;
- the electrical properties of the adhesive employed to glue the dielectric resonator to the ground plane [13];
- the deformation of the PCB, during the manufacturing process of the corporate feed network;
- an anechoic chamber required for exact measurements of the antenna array patterns was not available.

5. Conclusions

In this article the characteristics of a phase shifter capable of steering the main beam of the antenna array towards five predetermined directions, were demonstrated.

As shown in Table 3, a maximum beam steering angle of +36◦ was achieved, with this antenna architecture. In addition, a gain greater than 10 dB, was obtained at the maximum steering angle and a frequency of 5.35 GHz.

It was noticed that when the phase shifts were applied, the resonance frequency of the antenna array changed. This drift was compensated by using short open-circuit stubs placed on the phase shifter's lines. Using appropriate lengths of the short open-circuit stubs, the resonant frequency could be brought to the designed value.

Due to the compact size of the phase shifters, the antenna array is small (50 mm x 120 mm) and it can be inserted into small terminal devices, so that, the design can be employed in Wi-Fi and LTE technology.

In this paper, the switching between transmission lines of the phase shifter was achieved by placing a lumped component in each gap. In a future work PIN diode switches will be used to switch between the signal paths.

References

[1] K. Sarabandi, F. Wang, IEEE Transactions on Aerospace and Electronic Systems **43**(1), 251 (2007).
[2] T. Kinghorn, I. Scott, E. Totten, 2016 IEEE International Symposium on Phased Array Systems and Technology (PAST), 1 (2016).
[3] M. S. R. Bashri, T. Arslan, W. Zhou, 2015 Loughborough Antennas Propagation Conference (LAPC), 1 (2015).
[4] S. I. Latif, D. A. Nelson, V. La, 2016 17th International Symposium on Antenna Technology and Applied Electromagnetics (ANTEM), 1 (2016).
[5] Rudra L. Timsina, Richard A. Messner, Jean L. Kubwimana, Progress In Electromagnetics Research Symposium - Fall (PIERS - FALL), Singapore, 19–22 November, 1839 (2017).
[6] Nor Hidayu Shahadan, Mohd Haizal Jamaluddin, Muhammad Ramlee Kamarudin, Yoshihide Yamada, Mohsen Khalily, Muzammil Jusoh, Samsul Haimi Dahlan, IEEE Access, DOI:10.1109/ACCESS.2017.2760924, 22234 (2017).
[7] N. H. Shahadan, M. H. Jamaluddin, M. Hashim Dahri, M. R. Kamarudin, K. H. Yusof, 2018 International Symposium on Antennas and Propagation (ISAP 2018), October 23~26, 2018, Busan, Korea.
[8] Nipun K. Mishra, Soma Das, URSI AP-RASC 2019, New Delhi, India, 09 - 15 March 2019;
[9] L. P. Pontes, E. M. F. de Oliveira, C. P. N. Silva, A. G. Barboza, M. T. de Melo, Ignacio Llamas-Garro, Journal of Microwaves, Optoelectronics and Electromagnetic Applications **4**, 598 022);
[10] R. K. Mongia, P. Bhartia, International Jounal of Microwave and Millimeter-Wave Computer-Aided Engineering **4**(3), 230 (1994).
[11] J. C. Sethares, J. Naumann, IEEE Transactions on Microwave Theory &Techniques **14**(1), 2 (1996).
[12] Tang Xinyi, Dr. Phil. Thesis, National University of Singapore, 2011.
[13] I. Nicolaescu, A. G. Avădanei, S. B. Balmuș, J. Optoelectron. Adv. M. **14**(11-12), 1005 (2012).
[14] Mohammad Tariqul Islam, Waled Yousef Noor Aboaresh, Dinh Nguyen Quoc, Rabah W. Aldhaheri, Khalid Hamed Alharbi, Abdulah Jeza Aljohani, MD Samsuzaman, J. Optoelectron. Adv. M., **22**(11-12), 564 (2020).
[15] R. J. P. Douville, D. S. James, IEEE Transactions on Microwave Theory and Techniques, MTT-26 (3), 175 (1978).

*Corresponding author: gabryel21@yahoo.com